JOURNAL OF GEOPHYSICAL RESEARCH, VOL. 98, NO. B4, PAGES 6703–6714, APRIL 10, 1993

Earthquake Slip Vectors and Estimates of Present-Day Plate Motions

CHARLES DEMETS

University of Wisconsin at Madison

Although horizontal slip directions determined for earthquakes along transform faults and shallow subduction thrust faults are commonly assumed to parallel the direction of motion between two plates, systematic biases of earthquake slip vectors relative to the local long-term average plate direction can be introduced by a variety of causes, including deformation of forearcs above subduction zones, unmodeled lateral velocity heterogeneities near earthquake sources, and unrecognized changes in plate velocities within the averaging interval of the kinematic model. Given that earthquake slip vectors comprise nearly two thirds of the data used to derive the NUVEL-1 model for present-day global plate velocities, it is important to determine the extent to which potential systematic biases of earthquake slip vectors could degrade estimates of plate velocities given by NUVEL-1. Here, two alternative models for global plate velocities are derived and compared to NUVEL-1. The first model, NUVEL-SZ, is derived from a data set that omits the 240 subduction zone slip vectors in the NUVEL-1 data set but includes all remaining 882 kinematic data. The velocities predicted by NUVEL-SZ and NUVEL-1 differ little, with maximum differences of only 1 mm yr^{-1} and 2° along all plate boundaries except those surrounding the Caribbean plate. The second model NUVEL-G is derived from a data set that omits all 724 earthquake slip vectors but includes the remaining 277 spreading rates and 121 transform fault azimuths. Velocities predicted by NUVEL-G and NUVEL-1 also differ little, with maximum differences of 2 mm yr^{-1} and 4° except for the Caribbean plate boundaries. These results indicate that even in the unlikely event that all earthquake slip vectors in the NUVEL-1 data set are unreliable recorders of long-term plate directions, the slip vectors do not significantly degrade the model. It thus appears that the decision to use or not to use earthquake slip vectors to derive a global plate motion model has little practical effect on the ability to derive an accurate description of present-day plate velocities. Little emphasis is placed on the changes in estimates of Caribbean plate velocities that occur upon exclusion of earthquake slip vectors; nearly all of the data from Caribbean plate boundaries are suspect and it is unlikely that the NUVEL-SZ or NUVEL-G models represent a significantly improved description of Caribbean plate velocities. Comparison of 677 slip vectors from transform faults to directions predicted by NUVEL-G shows statistically insignificant differences along 12 of 15 spreading centers. The good agreement between the nearly instantaneous estimates of slip directions provided by slip vectors and the longer-term average directions given by NUVEL-G suggest that in general, transform fault slip vectors parallel the longer-term average directions along transform faults. Interestingly, a statistically significant difference between slip vectors from right-slipping and left-slipping transform faults is noted for nearly all spreading centers, with slip vectors along right-slipping and left-slipping faults rotated clockwise and counterclockwise, respectively, from the predicted direction. The cause of this bias is unknown, but may be related to biases introduced by unmodeled lateral heterogeneities in the mantle near transform faults.

INTRODUCTION

Earthquake focal mechanisms are arguably the most important source of information currently available for studies of instantaneous crustal deformation. Unlike other observations of present-day crustal stress and strain, which have limited geographic coverage and are repeated infrequently if at all, earthquakes provide a relatively continuous stream of information about globally distributed deformation. One of the most useful applications of earthquake focal mechanisms is for determining directions of motion along active plate boundaries. Strike-slip earthquakes along transform faults, and shallow-thrust earthquakes along subduction zone interfaces are generally assumed to have horizontal slip directions that parallel the local direction of motion between two plates. These slip directions have been used in conjunction with spreading rates and transform fault azimuths determined from magnetic and bathymetric observations to derive quantitative models for present-day global plate motions [*Minster et al.*, 1974; *Chase*, 1978; *Minster and Jordan*, 1978; *DeMets et al.*, 1990].

Paper number 92JB02868.
0148-0227/93/92JB-02868$05.00

Because the number of earthquake focal mechanisms has increased more rapidly over time than other kinematic measurements of plate motions, they now outnumber other types of data used to characterize global plate motions. For instance, the NUVEL-1 model, which describes the 3.0 m.y.-average velocities of 12 plates, is derived from 1122 spreading rates and slip directions, of which 724 or 65% are earthquake slip vectors [*DeMets et al.*, 1990]. Although the cumulative data importance of the 724 slip vectors, which is a measure of the information that the slip vectors contribute to the NUVEL-1 model [*Minster et al.*, 1974], constitutes less than 7% of the information contained in the 1122 data, they provide useful information about convergence directions across subduction zones, where alternative information about rigid plate convergence directions is not available.

The inexorable increase in the number of available earthquake focal mechanisms suggests that they will continue to contribute useful information to kinematic studies. It is thus important to identify the degree to which slip vectors satisfy the principal assumption underlying their use as kinematic data, namely, the assumption that slip vectors parallel long-term average plate directions. At least four potential sources of bias might skew earthquake slip directions away from the long-term average plate direction. These are plate boundary deformation that is distributed across multiple faults or other

structures, recent changes in plate directions, biasing of earthquake focal mechanisms due to unmodeled velocity heterogeneities in the upper mantle, and a slip-dependent bias along transform faults. Each is described briefly below.

The assumption that earthquake slip vectors parallel the long-term (i.e., several million year) slip directions between rigid plates depends in part on the degree to which slip along a single fault or series of closely spaced, similarly slipping faults accommodates all of the motion between two plates. Although this is probably an accurate assumption for strike-slip earthquakes that occur in transform fault valleys, where slip is concentrated along one or more parallel to subparallel fault strands, it is probably less accurate for subduction zones, where some of the relative motion between two converging plates is often accommodated by deformation inland from the main subduction thrust. Subduction-related deformation within the overlying plate ranges from shortening within foreland fold and thrust belts, to strike-slip faulting within forearcs in zones of oblique subduction, to rapid back-arc spreading. Rotation of subduction zone earthquake slip vectors away from the net rigid plate direction where such deformation occurs is well-documented. For instance, geologic and kinematic studies of subduction zones that accommodate oblique convergence find that slip vectors derived from shallow thrust earthquakes are often oriented between the trench-normal direction and the predicted convergence direction [*Fitch*, 1972; *Jarrard*, 1986; *DeMets et al.*, 1990]. The intermediate orientation of the subduction-related slip vectors implies that they record motion of the subducting plate relative to an overlying crustal sliver that is detached from the overlying rigid plate. Studies of forearc geology and seismicity [e.g. *Kimura*, 1986; *Geist et al.*, 1988; *Ekström and Engdahl*, 1989; *McCaffrey*, 1991; *DeMets*, 1992] suggest that oblique subduction occurs along most trenches and that earthquake slip vectors from subduction zones that accommodate oblique subduction should not be used to determine rigid plate convergence directions.

A second factor that determines whether slip vectors parallel the long-term direction of motion between two plates is the degree to which the direction of motion has changed over the averaging interval of the rigid plate velocity model. Most earthquakes release strain that has accumulated over one thousand year or less intervals, which is far shorter than the 3.0 m.y.-averaging interval of the NUVEL-1 model for present-day plate motions. Published plate motion models [*Chase*, 1978; *Minster and Jordan*, 1978; *DeMets et al.*, 1990] combine transform fault azimuths and earthquake slip vectors to constrain plate directions, and thus require the implicit assumption that plate directions have remained constant over the averaging interval of the model. If a recent change in plate velocities has occurred along one or more plate boundaries, earthquake slip vectors along these plate boundaries may differ systematically by an unknown amount from the longer-term average direction given by the transform fault strikes that are commonly used to constrain slip directions along spreading centers. C. DeMets and R. G. Gordon (manuscript in preparation, 1993) demonstrate that significant changes in spreading rates along 6 of 12 spreading centers appear to have occurred since 3.0 Ma, even after the spreading rates are adjusted for newly proposed changes in the geomagnetic reversal time scale [*Shackleton et al.*, 1990; *Baksi et al.*, 1992; *Spell and McDougall*, 1992]. Given that spreading rates along some plate boundaries appear to have changed, directions of motion along spreading centers, subduction zones, or both may also have changed.

A third potential source of systematic bias in earthquake focal mechanisms (and thus slip vectors) is direction-dependent wave front bending induced by subducting slabs or other lateral heterogeneities in the upper mantle [*Toksöz et al.*, 1971]. For example, *Engdahl et al.* [1977] demonstrate that unmodeled lateral mantle structure induces significant biases in first-motion focal mechanisms and slip vectors from the Aleutian subduction zone. Centroid moment tensors appear to be less susceptible to such biases given that they represent inversion of a variety of longer-period waveforms [*Ekström and Engdahl*, 1989; also T. Lay, D. Wiens, personal communications, 1992] and incorporate information about the relative wave amplitudes. The effect of near-source structure on slip vectors derived from focal mechanisms determined from first-motion studies or centroid moment tensor inversions also appears to depend on the orientation of the near-source structure relative to the surrounding seismographic network [*Engdahl et al.*, 1977].

A final, as-of-yet poorly understood source of bias is a systematic difference between earthquake slip directions along right- and left-slipping transform faults, first noted by *Argus et al.* [1989] for the Arctic and northern Atlantic ridges. *Argus et al.* [1989] find that slip vectors from right-slipping and left-slipping transform faults are rotated clockwise and counterclockwise respectively from the observed transform fault azimuths. If this slip-dependent bias occurs along other spreading centers, then directions predicted by a plate motion model for a plate boundary that has only right-slipping or left-slipping transform faults could be systematically biased relative to the true long-term slip direction. It is unclear whether this bias has a tectonic origin or is simply a by-product of direction-dependent wave front bending induced by anisotropic mantle velocities near ridges and transform faults.

In order to investigate the degree to which earthquake slip vectors affect the NUVEL-1 model, and to provide estimates of present-day plate velocities that are independent of earthquake slip vectors, two alternative models for present-day global plate motions are derived from subsets of the NUVEL-1 data. The first model, which is derived from a data set that excludes subduction zone slip vectors, is primarily intended to demonstrate that the 240 subduction zone slip vectors in the NUVEL-1 data set do not significantly affect the plate velocities predicted by NUVEL-1. The second model, which is derived from a data set that excludes all of the 724 earthquake slip vectors used to derive NUVEL-1, is a suitable reference model for kinematic studies that require plate velocity estimates that are unaffected by earthquake slip vectors. The latter model is used to seek evidence for biases in slip directions along spreading centers, and to investigate the aforementioned slip-dependent slip vector bias along transform faults.

Propagation of Systematic Errors in Rigid Plate Models

Much of the ensuing analysis requires some understanding of how systematic errors in data that are used to derive a closure-consistent rigid plate model can propagate through and degrade the model. The least squares inversion algorithm employed to derive NUVEL-1 and prior global plate motion models requires that all of the kinematic data used to derive the model be simultaneously fit in order to determine the set of Euler vectors that minimizes the total, weighted, least squares error

$$\chi^2 = \sum_{i=1}^{N} \left[\frac{d_i^{obs} - d_i^{pred}(\mathbf{m})}{\sigma_i} \right]^2 \quad (1)$$

where d_i^{obs} is the ith plate motion datum, d_i^{pred} is the model prediction for the ith plate motion datum, and σ_i is the standard error assigned to the ith datum. The model prediction is a function of the plate motion model, **m**, which consists of the Euler vectors describing the motion of each plate relative to a fixed plate. Least squares inversion of the data also yields information about the model covariances, which can be used to determine the uncertainties associated with individual Euler vectors, and data importances, which are useful for describing the amount of information contributed to the model by an individual datum [*Minster et al.*, 1974]. More detailed descriptions of the inversion algorithm and rate and azimuthal fitting functions are given by *DeMets et al.* [1990].

Simultaneous inversion of kinematic data from many plate boundaries guarantees that closure is satisfied for any given subcircuit within the global plate circuit (Figure 1). Given a sufficiently large set of data that are affected only by random errors, inversion of the data should yield a model that accurately predicts rigid plate velocities. However, if any subset of the data is systematically biased, every part of the model that is related to this subset of the data through plate circuit closures will be adversely affected. For example, if earthquake slip vectors from a given plate boundary do not parallel the long-term average plate direction, the least squares algorithm will seek the best compromise fit to the biased slip vectors and data from other plate boundaries. The degree to which biased slip vectors degrade the fit to data from other plate boundaries depends on the quantity, quality, and distribution of data from other plate boundaries. If data from other plate boundaries strongly constrain motion along the boundary with the biased slip vectors, then the slip vectors will be poorly fit and their effect on the remainder of the model will be small. The part of the systematic bias that propagates into the model will generally affect the model parameters that are poorly constrained or completely unconstrained by kinematic data.

Data Analysis

The analysis is divided into two parts. First, the 240 subduction zone slip vectors in the NUVEL-1 data set are eliminated and the remaining 882 data are inverted to determine a model free from biases that might be introduced by hard-to-detect deformation above subduction zones. The resulting model is compared to NUVEL-1 to determine how the two models differ. Second, all 724 slip vectors in the NUVEL-1 data set are eliminated, and the remaining 277 rates and 121 transform fault azimuths are used to derive a model free from any slip vector influence. The latter model is used to determine how the 724 slip vectors affect NUVEL-1.

Trench Slip Vectors and the NUVEL-1 Model

To derive a plate motion model that is completely

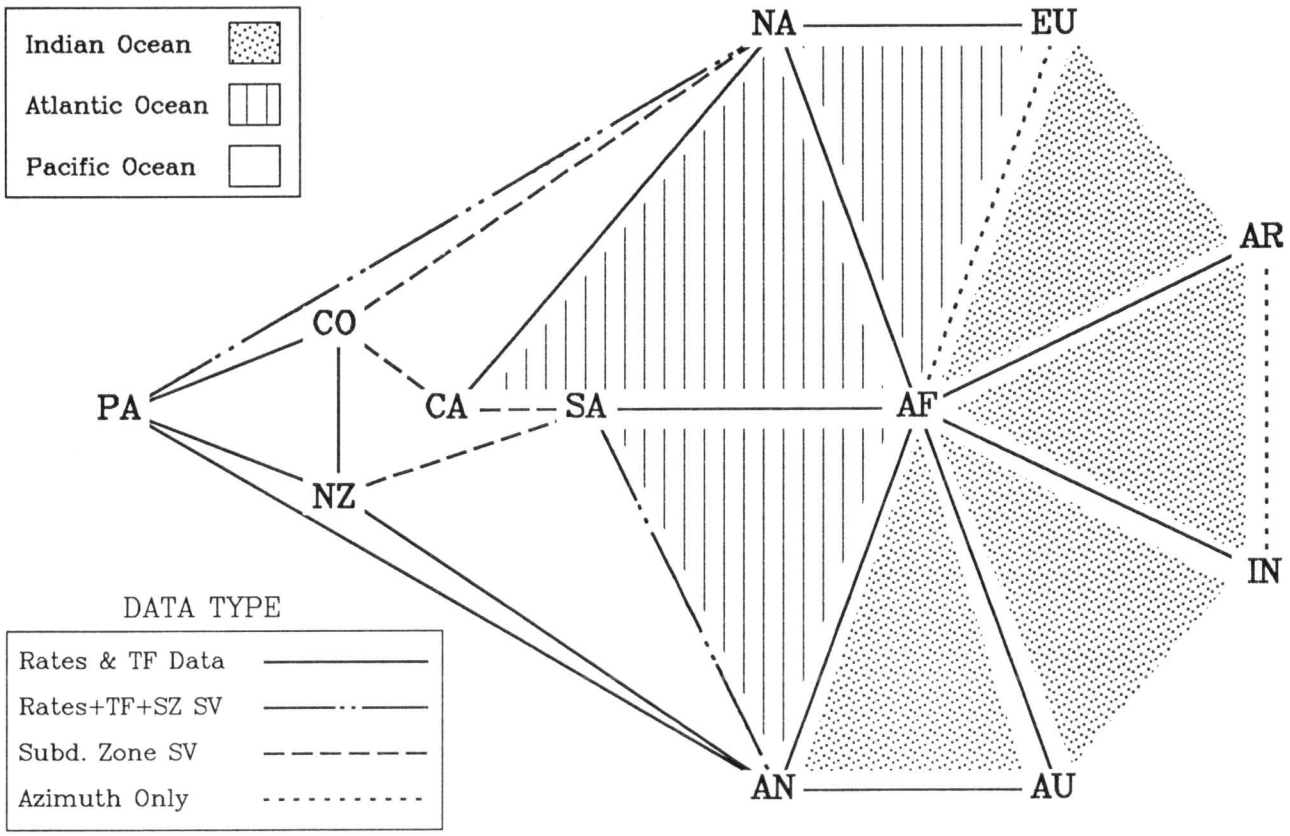

Fig. 1. The network of plate circuits that comprise the NUVEL-1 model. The 12 nodes represent plates whose velocities are modeled in NUVEL-1; the connecting lines represent their shared boundaries. Only plate boundaries that are represented in the NUVEL-1 data set and thus impose direct constraints on the NUVEL-1 model are shown. Abbreviations: subduction zone (SZ); transform fault (TF); Pacific plate (PA); Cocos plate (CO); Nazca plate (NZ); Caribbean plate (CA); South American plate (SA); North American plate (NA); Antarctic plate (AN); African plate (AF); Eurasian plate (EU); Australian plate (AU); Arabian plate (AR); and Indian plate (IN).

independent of the influence of subduction zone slip vectors, all of the NUVEL-1 data except for the 240 trench slip vectors included in the NUVEL-1 data were inverted to determine the set of Euler vectors that minimizes the least squares misfit. The 882 kinematic data used to determine the no-trench-slip-vector model consist of 277 spreading rates, 121 transform fault azimuths, and 484 other slip vectors. Hereafter, the model derived without any subduction zone slip vectors is referred to as NUVEL-SZ. As with NUVEL-1, the most compact model description consists of 11 Euler vectors and their covariances specified in a reference frame fixed to an arbitrarily specified 12th plate, which in this case is the Pacific plate. The Euler vectors and uncertainties for NUVEL-SZ are given in Table 1.

Statistical comparison. The F ratio test is used here to compare the fits of alternative models to various subsets of the 1122 NUVEL-1 data. As discussed in *Stein and Gordon* [1984],

$$F_{(d_2-d_1,\ N-d_2)} = \frac{\left[\chi^2(\text{model 1}) - \chi^2(\text{model 2})\right] / (d_2-d_1)}{\chi^2(\text{model 2}) / (N-d_2)} \quad (2)$$

where N is the number of data, d_1 and d_2 are the number of parameters used in model 1 and model 2 to fit the data, and χ^2 is defined in (1). The 99% confidence level is used as the cut-off point to indicate that the fits are significantly different.

The first question posed here is whether incorporation of the 240 trench slip vectors in the NUVEL-1 data set causes a significantly degraded fit of the NUVEL-1 model to the remaining 882 data. To test this, (2) is used to compare the respective fits of the two models to the 882 data. NUVEL-SZ fits the 882 data with $\chi^2 = 154.72$. For the same 882 data, NUVEL-1 gives $\chi^2 = 163.33$. Before applying (2) to test whether the models differ significantly, the value of $\chi^2 = 9.60$ for the 68 data from the Africa-India-Arabia plate circuit is subtracted from each of the above values of χ^2. This is necessary because the motions of the Indian and Arabian plates are isolated from the plate circuits that include the six plate boundaries with subduction zone slip vectors (Figure 1). The six model parameters and 68 data associated with the motions of India and Arabia do not therefore affect the fits of NUVEL-1 or NUVEL-SZ to data along plate boundaries that are linked through circuit closures to the six plate boundaries with subduction zone slip vectors. After adjusting for the model parameters and misfits associated with the Indian and Arabian plates, values of $\chi^2_{\text{NUVEL-SZ}} = 145.12$, $\chi^2_{\text{NUVEL-1}} = 153.73$, $\nu = 27$, and $N = 814$ are used in (2) to determine $F = 1.73$. This value of F exceeds the 95% confidence limit of $F = 1.5$ but is slightly less than the 99% threshold of $F = 1.8$ that would indicate that the fits of the two models differ at the 99% confidence level. Given that the 240 trench slip vectors only have a summed data importance of 2.22 in the NUVEL-1 model, which is less than 7% of the total importance of 33.0 contained in the data, it is not surprising that NUVEL-SZ does not differ significantly (at the 99% confidence level) from NUVEL-1.

For the 240 subduction zone slip vectors, the NUVEL-1 and NUVEL-SZ models give $\chi^2 = 98.41$ and $\chi^2 = 127.58$, respectively (Table 2). Nearly 80% of the difference in the values of χ^2 for the two models is accounted for by the difference in the models' fits to six slip vectors from the Lesser Antilles trench, which is assumed to record subduction of the South American plate beneath the Caribbean plate (Table 2). The average misfit to these six slip vectors increases from 15° for NUVEL-1 to 38° for NUVEL-SZ (Table 2). Along the five other plate boundaries with subduction zone slip vectors, the mean misfits of NUVEL-1 and NUVEL-SZ differ by a maximum angle of 1.8°. NUVEL-SZ thus fits the 240 trench slip vectors nearly as well as NUVEL-1, except for the Lesser Antilles trench slip vectors. The reasons for the degraded fit to the Lesser Antilles trench slip vectors are discussed in more detail below.

A practical estimate of the difference between NUVEL-1 and NUVEL-SZ. To determine how much the rates and directions predicted by NUVEL-SZ differ from those predicted by NUVEL-1, the velocities predicted by both models were compared at 48 locations from 25 plate boundaries. As summarized in Table 3, the differences in the velocities predicted by the two models are typically less than 1-2 mm yr^{-1} and 1°-2°, with the largest differences occurring along the boundaries of the Caribbean plate. In the Pacific basin, velocities differ by as much as 1.4 mm yr^{-1} and 2° along the Nazca-South America, Nazca-Antarctic, and Cocos-North America plate boundaries, but differ by less than 1 mm yr^{-1} and 1° elsewhere. For plate boundaries in the Arctic, Atlantic, and Indian ocean basins, velocities predicted by the two models differ at most by 0.6 mm yr^{-1} and 0.6°. Given the small differences between the velocities predicted by the two models, it appears that any bias introduced into NUVEL-1 by subduction zone slip vectors can probably be ignored by studies that require estimates of relative plate velocities not involving the Caribbean plate.

The Caribbean region: A nemesis of rigid plate models. Somewhat surprisingly, NUVEL-SZ fits trench slip vectors from the Cocos-North America and Pacific-North America plate boundaries better than NUVEL-1, even though NUVEL-1 was derived from a data set that included these data. To understand why this occurs, it is necessary to discuss the plate circuit closures that tie together the Cocos, Caribbean, North American, South American, and African plates (Figure 1).

One of the most difficult challenges for models of present-day plate motions has been to estimate the motion of the Caribbean plate relative to the adjacent North American,

TABLE 1. NUVEL-SZ Euler Vectors (Pacific Plate Fixed)

Plate Pair	Euler Vector λ† °N	Euler Vector ϕ† °E	Euler Vector ω, deg m.y.$^{-1}$	Error Ellipse σ_{max}	Error Ellipse σ_{min}	Error Ellipse ζ_{max}	Error Ellipse σ_ω, deg m.y.$^{-1}$
Africa	59.20	−73.10	0.968	1.2	1.0	76	0.012
Antarctica	64.39	−84.15	0.909	1.2	1.1	66	0.010
Arabia	59.66	−33.08	1.161	3.9	1.0	−88	0.020
Australia	60.10	1.77	1.123	1.0	1.0	58	0.016
Caribbean	61.70	−80.18	0.772	7.7	1.6	−4	0.046
Cocos	36.40	−108.89	2.116	1.0	0.6	−31	0.051
Eurasia	61.05	−85.09	0.901	1.3	1.2	73	0.016
India	60.50	−30.28	1.153	5.5	1.1	82	0.017
Nazca	54.34	−91.42	1.430	1.9	1.0	6	0.016
North America	48.68	−77.58	0.786	1.4	1.3	62	0.014
South America	55.20	−86.22	0.666	2.0	1.7	−80	0.012

† λ is latitude and ϕ is longitude.

Each named plate moves counterclockwise relative to the Pacific plate. One sigma-error ellipse is specified by the angular length of the semi-major and semi-minor axis and by the azimuth (ζ_{max}, given in degrees clockwise from north) of the major axis. The rotation rate uncertainty is determined from a one-dimensional marginal distribution, whereas the lengths of the principal axes are determined from a two-dimensional marginal distribution.

TABLE 2. Misfits to Subduction Zone Slip Vectors

Plate Pair	Number of Data	Mean Absolute Misfit, degrees*			Mean Misfit, degrees†			χ^2††		
		NU-1	NU-SZ	NU-G	NU-1	NU-SZ	NU-G	NU-1	NU-SZ	NU-G
Pa-Na	33	6.0	6.0	6.0	-1.2	-0.9	-1.3	8.54	8.51	8.54
Co-Na	44	8.6	8.4	8.4	-4.4	-2.7	-3.1	17.98	16.43	16.70
Co-Ca	56	9.3	10.0	9.9	2.5	4.1	3.9	23.50	25.40	25.16
Ca-Sa	6	15.7	38.3	35.5	-15.7	-38.3	-35.5	5.88	29.03	25.17
Nz-Sa	99	8.3	9.2	9.2	5.0	6.8	6.9	40.60	46.21	46.35
An-Sa	2	18.0	18.6	18.8	-18.0	-18.6	-18.8	1.91	2.00	2.05
All	240	8.5	9.6	9.5	1.1	2.0	2.0	98.41	127.58	123.97

* Mean absolute misfit is defined as a summation of the absolute values of the differences between the observed and predicted slip vector azimuths divided by the number of data.

† Mean misfit is defined as a summation of the differences between the observed and predicted slip vector azimuths divided by the number of data. Positive angles correspond to clockwise rotations of the slip vectors relative to the predicted direction.

†† χ^2 is defined by (1).

Abbreviations: NU-1 is NUVEL-1; NU-SZ is NUVEL-SZ; NU-G is NUVEL-G; Ca is Caribbean; Co is Cocos; Na is North America; Nz is Nazca; Pa is Pacific; Sa is South America.

TABLE 3. NUVEL-SZ and NUVEL-G Model Predictions Relative to NUVEL-1

Plate Pair	Coordinate, °N, °E	NU-SZ ΔRate*	NU-SZ ΔAz*	NU-G ΔRate†	NU-G ΔAz†	Plate Pair	Coordinate, °N, °E	NU-SZ ΔRate	NU-SZ ΔAz	NU-G ΔRate	NU-G ΔAz
Spreading Centers											
Pa-Na	24.5, 251.0	-0.6	-0.4	-0.3	-1.0	Af-Sa	15.8, 313.5	0.2	-0.6	0.1	-0.2
Pa-Co	8.9, 256.4	-0.1	0.6	0.0	0.5	Af-Sa	-17.0, 346.0	0.1	0.0	0.0	0.0
Pa-Nz	-13.1, 248.7	0.5	0.3	0.6	0.1	Af-Sa	-48.0, 350.0	-0.2	-0.1	-0.1	0.0
Pa-Nz	-32.0, 247.9	-0.8	0.3	-0.9	0.2	An-Sa	-58.9, 343.5	-0.1	0.0	-0.2	0.1
Pa-An	-41.9, 248.7	0.0	0.1	0.0	-0.3	Af-An	-52.2, 15.5	0.0	-0.1	0.2	0.0
Pa-An	-62.3, 204.0	0.0	0.2	-0.2	-0.6	Af-An	-32.5, 58.0	-0.1	0.2	0.2	-0.2
Pa-An	-63.2, 170.0	0.0	0.2	-0.1	-0.9	Au-An	-28.0, 74.0	-0.1	0.1	0.0	-0.8
Co-Nz	0.9, 272.0	0.0	-1.5	-0.1	-1.8	Au-An	-49.8, 110.2	-0.1	0.1	-0.1	-0.7
Nz-An	-37.8, 265.9	-1.2	1.6	-1.4	1.9	Au-An	-62.5, 157.8	-0.1	0.1	-0.2	-0.8
Eu-Na	67.9, 341.5	0.1	-0.1	0.0	0.1	Au-Af	-22.0, 68.0	0.0	0.0	-0.1	-0.8
Eu-Na	42.9, 330.9	0.1	0.0	-0.1	0.1	Au-Af	-12.0, 66.0	0.0	-0.1	0.0	-1.0
Af-Na	35.0, 323.5	-0.1	0.5	0.0	0.4	In-Af	1.4, 66.9	0.0	0.0	-0.2	-0.4
Af-Na	25.1, 314.6	0.1	0.6	0.2	0.5	In-Af	6.8, 60.0	0.0	0.0	0.1	-0.4
Ca-Na	19.0, 297.0	-3.2	-18.9	-3.2	-17.4	Ar-Af	12.1, 45.6	0.0	0.0	0.0	0.6
Subduction Zones											
Pa-Na	36.0, 239.5	-0.7	-0.1	-0.7	-0.1	Ca-Sa	12.1, 299.0	-2.0	-22.3	-2.2	-19.4
Pa-Na	58.4, 220.4	-0.6	0.4	-1.0	-0.2	Nz-Sa	-10.7, 281.4	0.4	1.9	0.1	1.9
Pa-Na	54.3, 199.8	-0.6	0.3	-0.9	-0.2	Nz-Sa	-20.3, 289.6	-0.3	2.0	-0.5	2.0
Pa-Na	51.6, 173.6	-0.5	0.3	-0.8	0.0	Nz-Sa	-30.0, 288.5	-0.7	1.8	-1.0	1.8
Pa-Na	47.9, 155.6	-0.4	0.3	-0.7	0.0	Nz-Sa	-38.5, 286.5	-1.2	1.7	-1.4	1.7
An-Sa	-50.0, 284.6	0.0	-0.5	-0.1	-0.8	Au-Pa	-20.0, 187.0	0.0	0.0	0.1	0.1
Co-Na	17.0, 261.3	-1.4	1.6	-1.7	1.2	Au-Pa	-35.0, 182.0	0.0	0.0	0.0	0.1
Co-Ca	13.0, 271.0	0.6	1.6	0.5	1.4	Au-Pa	-50.0, 163.0	0.0	0.0	-0.1	0.0
Other Plate Boundaries											
Af-Eu	37.0, 10.0	0.3	0.1	0.2	3.3	In-Au	-5.0, 87.0	0.1	-0.5	1.1	3.7
Ar-Eu	35.0, 47.0	0.6	0.3	0.5	1.4	In-Eu	30.7, 77.5	0.6	0.2	0.4	1.6

* ΔRate, which is in millimeters per year, and ΔAz, which is in degrees CW from north, are computed by subtracting the value predicted by NUVEL-SZ from that predicted by NUVEL-1.

† Computed by subtracting the rate and azimuth predicted by NUVEL-G from the rate and azimuth predicted by NUVEL-1.

Abbreviations: Af is Africa; An is Antarctic; Ar is Arabia; Au is Australia; Ca is Caribbean; Co is Cocos; Eu is Eurasia; In is India; Na is North America; Nz is Nazca; Pa is Pacific; Sa is South America.

South American, and Cocos plates. The boundaries of the Caribbean plate are in general kinematically complex, and it is therefore difficult to determine what constitutes a reliable measurement of the motion of the rigid portion of the Caribbean plate relative to the rigid interiors of the surrounding plates. For instance, recent evidence suggests that the Cayman spreading center, which is assumed by *DeMets et al.* [1990] to accommodate ~15 mm yr^{-1} of ~E-W opening between the Caribbean and North American plates, may be separated from the rigid interior of the Caribbean plate by an active fault that accommodates strike-slip motion [*Rosencrantz and Mann*, 1991]. The direction of Caribbean-North America motion east of the Cayman spreading center has also been a topic of debate (see *Stein et al.* [1988] for a discussion), and may deviate from the ~E-W direction incorporated into the NUVEL-1 data set.

Determination of the motion of the Caribbean plate with respect to South America is equally difficult. In the NUVEL-1 model, Caribbean-South America motion is directly constrained by six slip vectors that are derived from small earthquakes along the nearly aseismic Lesser Antilles trench. Seismicity along the Lesser Antilles trench appears to be dom-

inated by seismicity within the forearc, rather than along the subduction zone interface [*Stein et al.*, 1982]. It is thus possible that the six slip vectors record motion between the subducting South American plate and a complexly deforming forearc that is decoupled from the rigid Caribbean plate.

The lack of reliable kinematic data is responsible for much of the debate about published models for the motion of the Caribbean plate [*Jordan*, 1975; *Sykes et al.*, 1982; *Stein et al.*, 1988; *DeMets et al.*, 1990] and undoubtedly contributes to the inability of presently available models to fit data from the Caribbean boundaries while satisfying local plate circuit closures. The NUVEL-1 model gives a poor fit to data from the Caribbean-South America and Caribbean-North America plate boundaries, primarily because the Caribbean-South America slip vectors and Caribbean-North America data cannot both be fit without violating the circuit closure constraints imposed by data from other nearby plate boundaries. For instance, high-quality spreading rates and transform data from the Mid-Atlantic Ridge [*DeMets et al.*, 1990] constrain the relative motion between the North and South American plates via closure of the Africa-North America-South America circuit. Any model that attempts to fit the data from the Caribbean plate boundaries with North and South America must also satisfy the closure constraint imposed by the Africa-North America-South America circuit. Similarly, kinematic data within the Pacific-Cocos-North America-Caribbean plate circuit impose regional closure constraints that must be satisfied (Figure 1). As described above, any systematic bias in data from the Caribbean plate boundaries must be absorbed by the NUVEL-1 model through some combination of a misfit to the systematically biased data, and adjustment in the fit to data from other plate boundaries.

It is now possible to understand why NUVEL-SZ is able to fit the Pacific-North America and Cocos-North America trench slip vectors better than NUVEL-1, even though NUVEL-1 was derived from a data set that includes these slip vectors. Subduction zone slip vectors from the Cocos-Caribbean and Caribbean-South America plate boundaries are not used to derive NUVEL-SZ, thereby breaking the only direct closure constraints that must be satisfied in a model that links the Caribbean plate to the global plate circuit (Figure 1). Once the circuit closures that involve the Caribbean plate are broken, errors that were previously induced by the internally inconsistent Caribbean region kinematic data no longer propagate into the global plate circuit. Estimates of plate velocities within the Pacific-Cocos-Caribbean-North America and the Africa-North America-South America-Caribbean plate circuits, both of which are directly affected by incorporation of the Cocos-Caribbean and Caribbean-South America trench slip vectors, are no longer affected by the circum-Caribbean data. As a result, velocity predictions along the plate boundaries within these circuits, which include the Pacific-North America and Cocos-North America plate boundaries, are better able to adjust so as to optimize the fit to data within these circuits.

Once all subduction zone slip vectors are omitted from a global plate motion data set, the only data that link the Caribbean plate to the global plate circuit are from the Caribbean-North America plate boundary (Figure 1). If, as suggested above, some of the data that are used to estimate Caribbean-North America motion are biased, then the Caribbean plate velocities predicted by NUVEL-SZ must be considered suspect. The poor fit of the NUVEL-SZ model to the six Caribbean-South America slip vectors does not necessarily indicate that the six Lesser Antilles trench slip vectors do not record Caribbean-South America motion, but may instead indicate that the NUVEL-SZ Caribbean-North America Euler vector does not accurately model motion between these two plates.

Global Plate Motions Estimated Without Earthquake Slip Vectors

To determine how estimates of global plate velocities change if all slip vectors are omitted and only 3.0 m.y.-average spreading rates and transform fault azimuths are used to estimate present-day plate velocities, the 277 spreading rates and 121 transform fault azimuths in the NUVEL-1 data set are used to derive a no-slip vector model. Hereafter, this model is referred to as NUVEL-G(eological), with the reference to "NUVEL" retained to indicate the reliance of this model on the 398 NUVEL-1 data that are not earthquake slip vectors. Because the geological model is derived from a data set that omits all earthquake slip vectors, it can be used for studies that require plate velocity estimates that do not depend on earthquake slip vectors.

As with NUVEL-1, the geological model consists of 33 model parameters and their covariances, which completely describe the relative velocities of 12 plates. Table 4 gives the NUVEL-G Euler vectors and uncertainties in a reference frame fixed to the Pacific plate.

Spreading rates and transform fault strikes. Equation (2) is used to compare the fits of the NUVEL-1 and NUVEL-G models to the 398 spreading rates and transform fault azimuths. NUVEL-1 fits the 398 data with $\chi^2 = 86.654$. NUVEL-G, which gives the optimal least squares fit to these 398 data, gives $\chi^2 = 78.569$. For $\nu = 33$ and $N = 398$, $F = 1.1$, which is less than the threshold of $F = 1.7$ that would indicate that the fits of the two models differ at the 99% confidence level. Thus, NUVEL-1 and NUVEL-G provide nearly indistinguishable fits to the 398 data.

The velocities predicted by these two models differ by less than 1-2 mm yr^{-1} and 1°-2° along all spreading centers except the Cayman spreading center, which records opening along the complex Caribbean–North American plate boundary (Table 3). Thus, the decision to use or not to use earthquake slip vectors to derive a global plate motion model appears to have little practical effect on the ability to predict velocities along spreading centers.

This result is not unexpected given that the cumulative data importances of the 456 transform fault and 28 other slip vectors in the NUVEL-1 data set are only 2.647 and 1.613,

TABLE 4. NUVEL-G Euler Vectors (Pacific Plate Fixed)

Plate Pair	Euler Vector			Error Ellipse			
	λ* °N	ϕ* °E	ω, deg m.y.$^{-1}$	σ_{max}	σ_{min}	ζ_{max}	σ_ω, deg m.y.$^{-1}$
Africa	58.81	−73.19	0.968	1.5	1.3	−50	0.012
Antarctica	63.87	−83.66	0.907	1.5	1.4	−53	0.011
Arabia	59.34	−33.70	1.157	3.8	1.3	−89	0.020
Australia	60.13	1.84	1.121	1.4	1.0	40	0.017
Caribbean	60.58	−80.22	0.782	7.6	1.7	−5	0.051
Cocos	36.43	−108.86	2.113	1.0	0.8	−25	0.054
Eurasia	60.73	−84.98	0.904	1.6	1.4	-52	0.020
India	60.39	−28.99	1.154	6.2	1.4	82	0.019
Nazca	54.12	−91.28	1.431	2.1	1.2	5	0.016
North America	48.25	−77.65	0.787	1.8	1.4	−33	0.014
South America	54.55	−85.83	0.665	2.5	2.0	−56	0.013

* See Table 1.

respectively, out of a total model importance of 33.0. As was the case with the 240 subduction zone slip vectors, neither of these data subsets contributes a substantial amount of information to the NUVEL-1 plate circuit closures.

Transform fault slip vectors. Interestingly, the NUVEL-G model fits the 456 transform fault slip vectors in the NUVEL-1 data set nearly as well as NUVEL-1, even though these data were not used to derive the NUVEL-G model. On average, the 456 slip vectors are rotated 0.4° counterclockwise (CCW) from the directions predicted by NUVEL-1, and 0.5° CCW from the directions predicted by NUVEL-G (Figure 2, Table 5), with nearly all of this small bias concentrated along the easternmost part of the Australia-Antarctic spreading center and the Pacific-Antarctic rise. Thus, the fit of the two models to these data differs on average by only 0.1° (Table 5).

Subduction zone slip vectors. For the six subduction zone plate boundaries considered here, NUVEL-G predicts convergence directions and rates that are nearly identical to those predicted by NUVEL-1 and NUVEL-SZ (Table 3). The largest difference between the velocities predicted by the two models is along the Caribbean-South America boundary; however, for reasons given above, it is unclear whether this difference is physically significant. Overall, the NUVEL-G model fits the 240 subduction zone slip vectors better than NUVEL-SZ (Table 2), with nearly all of the improvement attributable to the fact that NUVEL-G fits the six trench slip vectors along the Lesser Antilles trench slightly better than NUVEL-SZ.

How Well Do Slip Vectors Agree with Long-Term Average Plate Directions?

Given that the NUVEL-G model provides an estimate of long-term average plate directions independent of information from earthquake slip vectors, it can be used as a reference model for comparison to slip directions determined from transform fault earthquakes, which average slip directions over a shorter interval. "Long-term" is used here to describe any interval longer than the ~1000 year or less averaging interval of a typical transform fault slip vector. In order to exploit all available information about instantaneous slip directions along spreading centers, the 456 transform fault slip vectors in the NUVEL-1 data set are supplemented by 221 additional transform fault slip vectors taken from Harvard centroid-moment tensor solutions [e.g., Dziewonski et al., 1990] for the period July, 1987 through September, 1991. The criterion for selecting and assigning uncertainties to the 221 new slip vectors are identical to those used to select the 456 transform fault slip vectors in the NUVEL-1 data set [*DeMets et al.*, 1990]. The 677 slip vectors represent a relatively complete sampling of large transform fault earthquakes that have occurred since 1963 along the 15 spreading centers represented in the NUVEL-1 data set.

On average, the 677 transform fault slip vectors are rotated 0.04 standard deviations CCW relative to the directions predicted by NUVEL-G (Figure 2). This corresponds to an average CCW rotation of the slip vectors of only 0.6° relative to the long-term average direction. As discussed above, much of this difference is concentrated in slip vectors from the Australia-Antarctic and Pacific-Antarctic spreading centers, which have a mean weighted residual of -0.14 standard deviations. In contrast, the remaining 472 slip vectors have a mean of 0.01 standard deviations.

To determine whether the long-term average slip directions predicted by NUVEL-G agree with the shorter-term average transform fault earthquake slip directions for each of the 15 spreading centers, (2) was used to compare the fit of the NUVEL-G model to the fit of an Euler pole that optimizes the least squares fit to transform fault slip vectors from each of the 15 plate boundaries. NUVEL-G fits slip vectors from 12 of the 15 spreading centers as well as the best fitting Euler poles (Figure 3; Table 5).

As shown in Figure 3, NUVEL-G fits slip vectors from the Australia-Antarctica, Eurasia-North America, and Australia-Africa plate boundaries significantly worse than their corresponding best fitting Euler poles (Table 5). Several lines of evidence suggest that the difference between the observed and predicted directions along the Australia-Antarctic boundary is caused by slow deformation of the Australian plate west of the Macquarie Ridge Complex, and east of the Balleny, Tasman, and George V transform faults along the eastern Southeast Indian ridge [*DeMets et al.*, 1988]. First, slip vectors from the Australia-Antarctic spreading center agree well with the direction predicted by NUVEL-G everywhere except along the easternmost Southeast Indian ridge near the Australia-Antarctic-Pacific triple junction. Along this section of the ridge, both the transform fault azimuths and the slip vectors are rotated CCW from the direction predicted by NUVEL-G. Moreover, significant seismicity occurs within this salient of the Australian plate [*Stewart*, 1983], which suggests that it may move slowly relative to the rigid interior of the Australian plate. To test the hypothesis that the discrepancy between the observed and predicted slip directions along the Australia-Antarctica spreading center is primarily attributable to deformation of the Australian plate immediately west of the Macquarie Ridge Complex, 71 slip vectors from the transform faults located east of 138°E were omitted and the least squares fit of an Euler pole that best fits the remaining 54 Australia-Antarctic slip vectors was compared to the fit of the NUVEL-G Australia-Antarctic Euler vector. For this case, (2) gives $F = 0.1$, far less than the value of $F = 5$ that would indicate a significant difference at the 99% confidence level. The Australia-Antarctic slip vector bias indicated in Figure 3 thus appears to be isolated to the azimuthal data from the tectonically suspect region near the Macquarie triple junction.

For the Australia-Africa and Eurasia-North America plate boundaries, there are no obvious tectonic explanations for the differences between the short-term and predicted long-term directions; however, the observed discrepancies appear to fit into an intriguing but unexplained pattern observed by *Argus et al.* [1989] for transform fault slip vectors along the Africa-North America and Eurasia-North America plate boundaries. This pattern, which emerges when slip vectors are categorized as right-slipping or left-slipping, is described in more detail below.

Right- and Left-slipping Transform Faults: Evidence for a Systematic Bias in Transform Fault Slip Vectors

In a detailed study of 3.0 m.y.-average plate velocities of the Africa-Eurasia-North America plate circuit, *Argus et al.* [1989] document evidence for a curious discrepancy between transform fault slip vectors located along right- and left-slipping transform faults from the Africa-North America and Eurasia-North America plate boundaries. Along these two

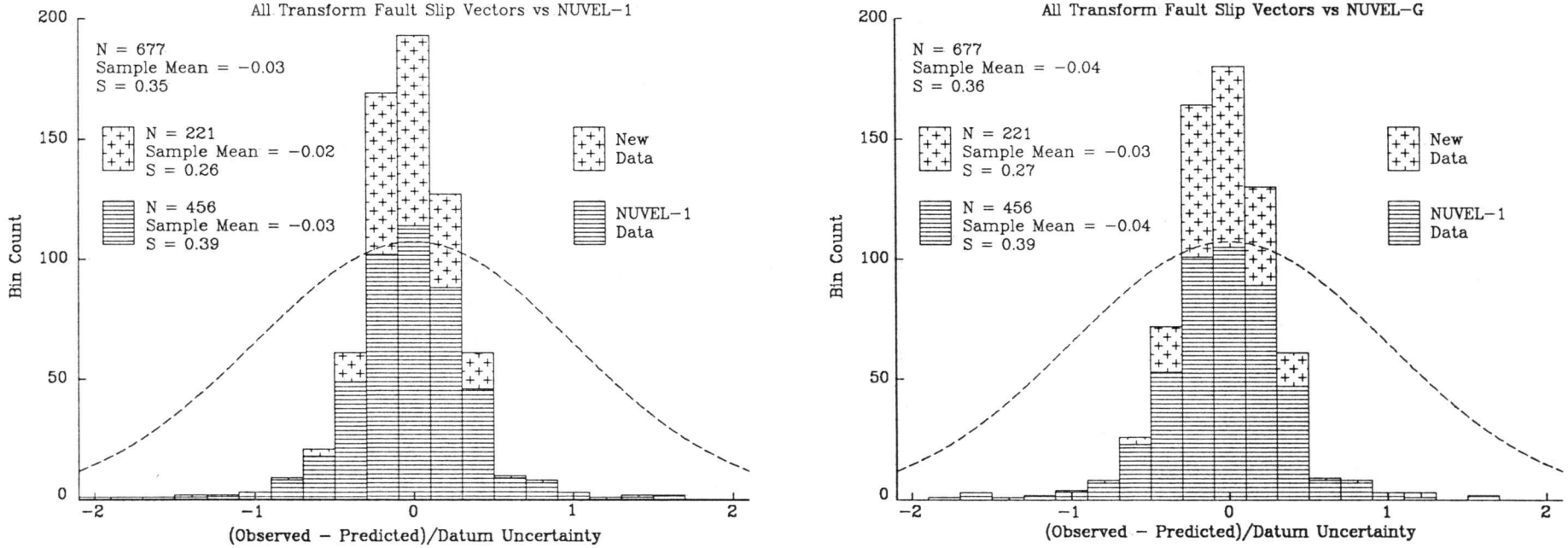

Fig. 2. Histograms of the normalized residual azimuths between the 677 transform fault slip vectors and the directions predicted by the NUVEL-1 and NUVEL-G models. Errors are normalized by dividing the angle between a slip vector and predicted direction by the uncertainty assigned to the slip vector. A positive error indicates that the slip vector is oriented clockwise from the predicted azimuth. "S" represents the sample standard deviation of the normalized errors. Dashed curves show the Gaussian distribution of errors expected if the data uncertainties were properly estimated. The computed sample standard deviations are less than unity, showing that the slip vector uncertainties were systematically overestimated. (Upper Left) Directions predicted by NUVEL-1 relative to the 456 NUVEL-1 transform fault slip vectors and the 221 new slip vectors. (Upper Right) Directions predicted by NUVEL-G relative to the 456 NUVEL-1 transform fault slip vectors and the 221 new slip vectors.

TABLE 5. Misfits to 677 Transform Fault Slip Vectors

Plate Pair	Number of Data	Mean Absolute Misfit, deg*		Mean Misfit, deg*		χ^{2}*		
		NU-1	NU-G	NU-1	NU-G	NU-1	NU-G	Best Fit†
Af-An	46	3.3	3.3	0.4	0.3	4.13	4.13	4.13
Af-In	11	5.5	5.2	5.1	4.6	2.08	1.98	1.65
Af-Ar	9	4.2	4.6	3.6	4.1	0.48	0.56	0.22
Af-Na	18	2.4	2.2	-1.6	-1.2	0.84	0.72	0.49
Af-Sa	139	3.6	3.6	0.4	0.4	9.86	9.77	9.38
An-Pa	80	4.5	4.7	-2.1	-2.6	8.17	8.59	7.68
An-Sa	12	4.2	4.2	0.0	0.1	1.69	1.69	1.47
Au-Af	27	4.2	4.7	-2.6	-3.5	1.71	2.11	1.30
Au-An	125	5.7	6.0	-2.1	-2.8	22.97	24.55	18.69
Eu-Na	20	4.1	4.1	3.0	3.1	1.31	1.34	0.62
Co-Nz	27	5.2	5.6	-0.5	-2.2	4.23	4.43	3.84
Nz-An	73	4.4	5.3	0.1	1.9	11.89	12.09	11.01
Nz-Pa	40	5.7	5.7	-1.9	-1.7	8.18	8.16	8.15
Pa-Co	11	3.3	3.0	-1.0	-0.4	0.37	0.34	0.30
Pa-Na	39	4.8	4.6	2.3	1.2	4.87	4.97	4.64
NUVEL-1	456	4.5	4.6	-0.4	-0.5	67.62	69.20	
New	221	4.5	4.7	-0.5	-0.75	15.16	16.25	
All	677	4.5	4.7	-0.4	-0.6	82.78	85.45	

* See Table 2 for description and Table 3 for abbreviations.
† Optimal least-squares fit to transform fault slip vectors.

plate boundaries, slip vectors along left-slipping transform faults are rotated several degrees CCW from the observed transform fault trends, and slip vectors along right-slipping transform faults are rotated several degrees clockwise (CW) from the observed transform fault trends.

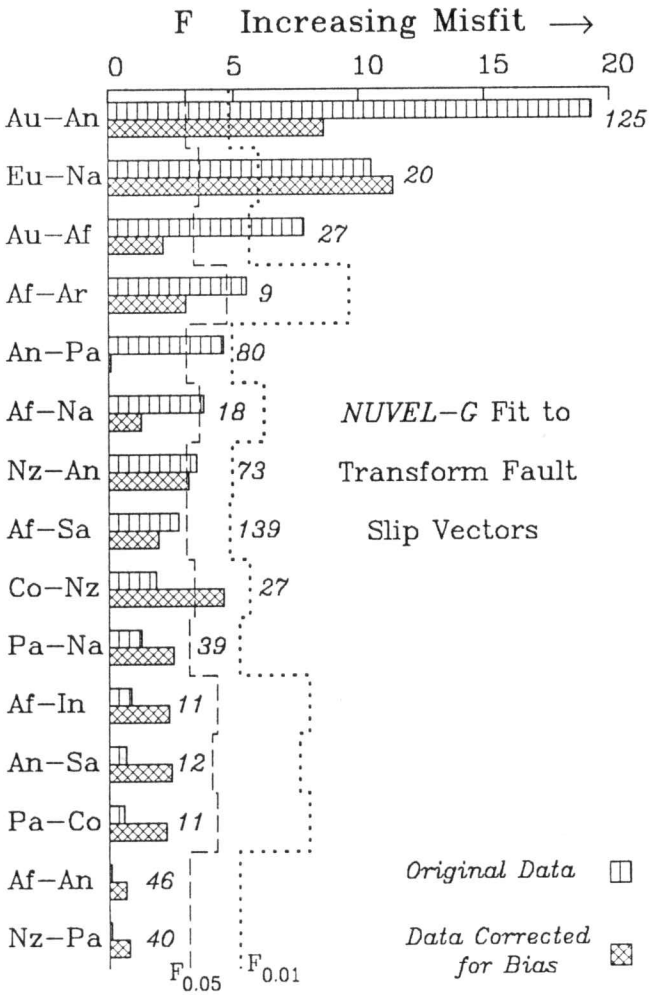

To determine whether a similar bias occurs along other spreading centers, the 677 transform fault slip vectors described above were divided into two subsets corresponding to right-slipping and left-slipping transform faults, and were compared separately to the directions predicted by NUVEL-G. The results strongly support the pattern observed by *Argus et al.* [1989] (Figure 4). Of the 12 spreading centers with left-slipping transforms, 10 spreading centers have slip vectors that are rotated CCW from the predicted directions, and only one spreading center, the Africa-India plate boundary, has slip vectors that are rotated CW from the slip direction predicted by NUVEL-G. Given that the Africa-India direction predicted by NUVEL-G may be in error by several degrees since it is only weakly constrained by mapped transform fault strikes and plate circuit closures, little significance is attributed to the apparent CW rotation of the Africa-India slip vectors. Of the 12 spreading centers with right-slipping transform faults, seven show CW biases significantly greater than 0°; four show no bias; and only one, the Cocos-Nazca spreading center, has slip vectors that are rotated CCW from the predicted direction (Figure 4). The Cocos-Nazca slip vectors may also be a special case because 19 of the 23 slip vectors that deviate from the observed pattern are located along the Panama fault, which differs from other transform faults in that it connects a spreading center to a trench rather than another ridge segment. On average, slip vectors located on right-slipping transforms are rotated 1.2° CW from the predicted direction, and slip vectors

Fig. 3. Tests for significant differences between transform fault slip vectors from 15 spreading centers and directions predicted by NUVEL-G. Horizontal axis shows values of F computed from (2) and values of χ^2 given in Table 5. F increases as the discrepancy between the predicted and observed slip directions increases. Numbers to the right of the shaded bars represent the number of slip vectors from the spreading center. Dashed and dotted lines represent the 95% and 99% cut-off values for significant differences between the predicted and observed directions. For each spreading center, slip vectors have also been corrected by the slip-dependent bias, and the fit of the Euler pole that best fits the bias-corrected slip vectors has been compared to the fit of the NUVEL-G Euler pole. Abbreviations for plate names follow those given in Table 2.

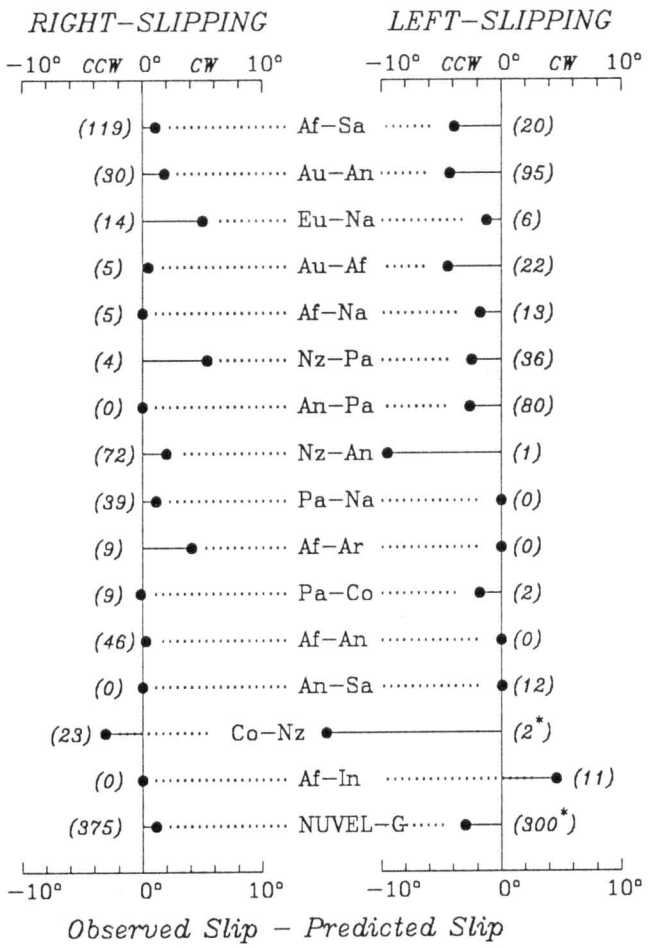

Fig. 4. Transform fault slip vectors relative to directions predicted by NUVEL-G as a function of the sense of slip along a transform fault. CW and CCW refer to sense of rotation of the slip vectors relative to the predicted directions. The numbers in parentheses indicate the number of slip vectors that are used to determine the mean bias. An asterisk indicates that two slip vectors from the Cocos-Nazca spreading center near the Galapagos microplate are not included in this part of the analysis because of uncertainty about their tectonic setting. The number of slip vectors is thus two less than for other parts of the analysis. Abbreviations for plate names follow those given in Table 2.

located on left-slipping transforms are rotated 3.0° CCW from the predicted direction (Figure 4).

If the slip vectors associated with right-slipping and left-slipping transform faults are treated as separate data populations with independent means and distributions, then slip vectors from right-slipping and left-slipping transform faults should have significantly different mean directions relative to the directions predicted by NUVEL-G. An appropriate statistical test for the comparison of two large-sample distributions of measurements is the two-sample z test [*Book*, 1977]

$$z = \frac{\bar{E}_R - \bar{E}_L}{\left[\frac{S_R^2}{n_R} + \frac{S_L^2}{n_L}\right]^{\frac{1}{2}}} \tag{3}$$

where $\bar{E}_L$ and $\bar{E}_R$ are the mean weighted differences of the left- and right-slipping slip vectors from the directions predicted by NUVEL-G, S_L and S_R are the sample standard deviations of the differences associated with left- and right-slipping slip vectors, and, n_L and n_R are the number of left- and right-slipping slip vectors.

For the 300 left-slipping transform slip vectors, $\bar{E}_L = -0.16$ standard deviations, with a standard deviation of $S_L = 0.372$ (Figure 5). For the 375 right-slipping slip vectors, the bias is $\bar{E}_R = 0.05$ standard deviations, with a standard deviation of $S_R = 0.335$ (Figure 5). Two slip vectors from the Cocos-Nazca plate boundary have been omitted from this part of the analysis because of uncertainty about their tectonic setting. Equation (3) gives $z = 7.6$, which is higher than the 99% value of $z = 2.3$ expected for two data populations that have means and distributions that are statistically different. This suggests that the difference between slip vectors along right- and left-slipping transforms is significant, even though the means of the two populations of slip vectors differ by only ~4° relative to the directions predicted by NUVEL-G.

As discussed above, some or all of the observed ~5°-7° CCW rotation of the 71 Australia-Antarctic slip vectors from transform faults near the Pacific-Antarctic-Australia triple junction may be attributable to slow deformation of the Australian plate west of the Macquarie ridge complex. If these 71 slip vectors are omitted and the above analysis is repeated, $\bar{E}_L = -0.12$ and $S_R = 0.392$ standard deviations. Equation (3) then gives $z = 5.5$, which indicates that the mean biases for right-slipping and left-slipping transform fault slip vectors are still significantly different at the 99% confidence level.

Most spreading centers have a mixture of left-slipping and right-slipping transforms, which makes it likely that the effect of a small systematic bias of slip vectors along left-slipping transforms will be largely cancelled by the opposite sense bias along right-slipping transform faults. However, along plate boundaries where all or nearly all of the transform faults have the same sense of slip (e.g., Nazca-Antarctic, Pacific-Antarctic, Australia-Africa), a systematic difference of 1°-3° between measured transform fault azimuths and transform fault slip vectors could explain why the directions predicted by NUVEL-G and those predicted by the Euler poles that best fit the transform slip vectors sometimes differ (see previous section).

To test this possibility, a counterclockwise correction of 0.05 standard deviations, corresponding to the mean standard deviation computed for the 375 right-slipping transform fault slip vectors, was applied to each of the transform fault slip vectors from right-slipping transforms. Similarly, a clockwise correction of 0.12 standard deviations was applied to each of the 229 left-slipping transform fault slip vectors (the 71 Australia-Antarctic slip vectors from near the Macquarie triple junction were not used to determine the mean bias of 0.12 standard deviations because of the evidence for a tectonic bias in these data). Best fitting Euler poles for each of the 15 plate boundaries were redetermined using the corrected slip vectors, and the directions predicted by the revised best fitting Euler poles were again compared to the directions predicted by NUVEL-G using (2). After correction for the slip-dependent bias, the previously observed discrepancy along the Australia-Africa plate boundary is eliminated. The discrepancy along the Australia-Antarctic plate boundary is reduced (Figure 3), and if the 71 slip vectors from near the Macquarie triple junction are omitted and the analysis is repeated, the entire discrepancy along this plate boundary is eliminated. The only remaining significant difference between the longer-term average directions predicted by NUVEL-G and the short-term

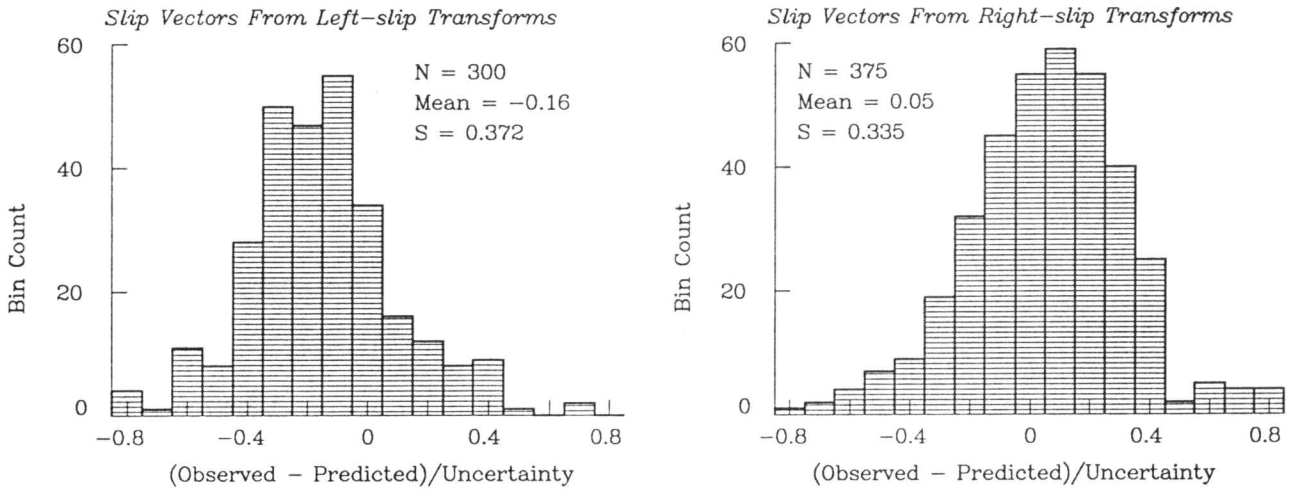

Fig. 5. Distribution of the weighted, residual differences between slip vector directions along right- and left-slipping transform faults, and directions predicted by the NUVEL-G model. A positive error indicates that the slip vector is oriented clockwise from the predicted azimuth.

directions given by the earthquake slip vectors is along the Eurasia-North America plate boundary.

One possible explanation for the systematic difference between the predicted and bias-corrected slip directions from the Eurasia-North America plate boundary is that the direction of motion between the Eurasian and North America plates may have rotated clockwise over the past 3.0 million years. An analysis of very long baseline interferometry (VLBI) measurements between the Eurasian and North American plates indicates that the instantaneous direction is oriented clockwise from the long-term average direction (D. Argus and R. G. Gordon, manuscript in preparation, 1993); however, the Eurasia-North America direction determined from VLBI is poorly determined for the Arctic region and does not differ significantly from the direction predicted by NUVEL-G. Until the accuracy of space-based measurements of plate motion improves, it may be premature to ascribe the discrepancy observed along this spreading ridge to a recent change in the Eurasia-North America direction.

Assuming that the observed slip-dependent bias is not an unlikely statistical artifact that will disappear as more slip vectors become available, it is unclear why slip vectors along transform faults with opposite senses of slip are rotated relative to the predicted direction. It seems unlikely that recent changes in plate directions could explain the bias because slip vectors along right- and left-slipping transforms are observed to rotate in opposite senses instead of in the same sense, as should be observed following a change in plate direction. The bias may arise if earthquakes in the transform fault valley tend to rupture faults that are subparallel to the slip direction [*Argus et al.*, 1989]. An equally plausible explanation advanced by *Argus et al.* is the possibility that small biases in earthquake focal mechanisms are induced by lateral variations in shallow mantle structure near transform faults. Given that the observed rotation of slip vectors relative to the predicted slip direction is only 1°–2°, small changes in the waveform paths and amplitudes due to variations in upper mantle seismic velocities near ridges might cause a small bias in centroid moment tensor inversions of transform fault earthquake data. Unfortunately, no systematic studies of the effect of a realistic near-ridge velocity structure combined with the present global seismic station geometry have appeared in the literature. It is therefore difficult to assess whether the observed slip vector bias could be attributed to this effect.

Given that NUVEL-1 and NUVEL-G predict present-day plate velocities that are statistically indistinguishable, it appears that the systematic differences between slip vectors from right- and left-slipping transform faults have little effect on estimates of global plate velocities. Along plate boundaries where all or nearly all of the transform faults have the same sense of slip, the 1°–3° discrepancy between the slip vectors and the longer-term average transform fault azimuths could eventually degrade the rigid-plate velocity model predictions if enough earthquake slip vectors were used to derive the model. However, any such effect is likely to be offset by the increasing number of highly accurate transform fault azimuths available from multibeam surveys of transform faults, which impose strong constraints on the long-term average rigid plate directions in global plate motion models.

Conclusions

Elimination of the 240 subduction zone vectors incorporated in the NUVEL-1 data set yields a modified global plate motion model that predicts velocities that differ by only 1 mm yr^{-1} and 2° from velocities predicted by NUVEL-1, except for the boundaries of the Caribbean plate. Elimination of all slip vectors from the data set used to derive the NUVEL-1 model and reinversion of the remaining 3.0 m.y.-average spreading rates and transform fault azimuths yields a model, NUVEL-G, that predicts plate velocities that differ by only 0–2 mm yr^{-1} and 0°–4° along all plate boundaries except those bordering the Caribbean plate. Thus, even in the unlikely event that all of the slip vectors incorporated in the NUVEL-1 data set are unreliable measures of rigid plate directions, the slip vectors do not significantly alter the velocities estimated by NUVEL-1. Long-term average plate directions predicted by NUVEL-G along 12 of the 15 spreading centers do not differ significantly from the shorter-term average directions derived from earthquake slip vectors. The average difference between the predicted long-term and observed short-term directions is less than 1° globally, which indicates that on average, transform fault slip vectors give an excellent approximation to present-day plate directions. A significant difference between the predicted and observed slip directions along the Southeast

Indian Ridge appears to be related to slow deformation of the Australian plate west of the Macquarie Ridge Complex. The slip-dependent bias that has been previously identified along right-slipping and left-slipping transform faults in the North Atlantic and Arctic appears to occur along nearly all spreading centers. This bias may be an artifact of biases in focal mechanisms that may be induced by near-ridge seismic velocity variations; however, this assertion is unproven and remains a topic of future research.

Acknowledgments. The author thanks Clem Chase, Jean Lin, and Peter Shaw for constructive reviews. This research began at the Naval Research Laboratory under a National Research Council grant, continued at the Jet Propulsion Laboratory, California Institute of Technology, under a contract with NASA, and was supported at U.W.-Madison under NSF grant EAR 9205083.

References

Argus, D. F., R. G. Gordon, C. DeMets, and S. Stein, Closure of the Africa-Eurasia-North America plate motion circuit and tectonics of the Gloria fault, *J. Geophys. Res., 94,* 5585–5602, 1989.

Baksi, A. K., V. Hsu, M. O. McWilliams, and E. Farrar, $^{40}Ar/^{39}Ar$ dating of the Brunhes-Matuyama geomagnetic field reversal, *Science, 256,* 356–357, 1992.

Book, S. A., Statistics, 511 pp., McGraw Hill, New York, 1977.

Chase, C. G., Plate kinematics: The Americas, East Africa, and the rest of the world, *Earth Planet. Sci. Lett., 37,* 355–368, 1978.

DeMets, C., R. G. Gordon, and D. F. Argus, Intraplate deformation and closure of the Australia-Antarctica-Africa plate circuit, *J. Geophys. Res., 93,* 11,877–11,897, 1988.

DeMets, C., Oblique convergence and deformation along the Kuril and Japan trenches, *J. Geophys. Res., 97,* 17,615–17,625, 1992.

DeMets, C., R. G. Gordon, D. F. Argus, and S. Stein, Current plate motions, *Geophys. J. Inter., 101,* 425–478, 1990.

Dziewonski, A. M., G. Ekström, J. H. Woodhouse, and G. Zwart, Centroid-moment tensor solutions for October-December 1989, *Phys. Earth Planet. Inter., 62,* 194–207, 1990.

Ekström, G., and E. R. Engdahl, Earthquake source parameters and stress distribution in the Adak Island Region of the Central Aleutian Islands, Alaska, *J. Geophys. Res., 94,* 15,499–15,519, 1989.

Engdahl, E. R., N. H. Sleep, and M. T. Lin, Plate effects in North Pacific subduction zones, *Tectonophysics, 37,* 95–116, 1977.

Fitch, T. J., Plate convergence, transcurrent faults, and internal deformation adjacent to Southeast Asia and the western Pacific, *J. Geophys. Res., 77,* 4432–4460, 1972.

Geist, E. L., J. R. Childs, and D. W. Scholl, The origin of summit basins of the Aleutian Ridge: Implications for block rotation of an arc massif, *Tectonics, 7,* 327–341, 1988.

Jarrard, R. D., Terrane motion by strike-slip faulting of forearc slivers, *Geology, 14,* 780–783, 1986.

Jordan, T. H., The present-day motions of the Caribbean plate, *J. Geophys. Res., 80,* 4433–4439, 1975.

Kimura, G., Oblique subduction and collision: Forearc tectonics of the Kuril arc, *Geology, 14,* 404–407, 1986.

McCaffrey, R., Slip vectors and stretching of the Sumatran fore arc, *Geology, 19,* 881–884, 1991.

Minster, J. B., and T. H. Jordan, Present-day plate motions, *J. Geophys. Res., 83,* 5331–5354, 1978.

Minster, J. B., T. H. Jordan, P. Molnar, and E. Haines, Numerical modeling of instantaneous plate tectonics, *Geophys. J. R. astron. Soc., 36,* 541–576, 1974.

Rosencrantz, E., and P. Mann, SeaMARC II mapping of transform faults in the Cayman Trough, Caribbean Sea, *Geology, 19,* 690–693, 1991.

Shackleton, N. J., A. Berger, and W. R. Peltier, An alternative astronomical calibration of the lower Pleistocene timescale based on ODP Site 677, *Trans. R. Soc. Edinburgh Earth Sci., 81,* 251–261, 1990.

Spell, T. L., and I. McDougall, Revisions to the age of the Brunhes-Matuyama boundary and the Pleistocene geomagnetic polarity timescale, *Geophys. Res. Lett., 19,* 1181–1184, 1992.

Stein, S., and R. G. Gordon, Statistical tests of additional plate boundaries from plate motion inversions, *Earth Planet. Sci. Lett., 69,* 401–412, 1984.

Stein, S., J. F. Engeln, D. A. Wiens, K. Fujita, and R. C. Speed, Subduction seismicity and tectonics in the Lesser Antilles arc, *J. Geophys. Res., 87,* 8642–8664, 1982.

Stein, S., C. DeMets, R. G. Gordon, J. Brodholt, J. F. Engeln, D. A. Wiens, D. Argus, P. Lundgren, C. Stein, and D. Woods, A test of alternative Caribbean plate relative motion models, *J. Geophys. Res., 93,* 3041–3050, 1988.

Stewart, L. M., Strain release along oceanic transform faults, Ph. D. thesis, Yale University, New Haven, Conn., 1983.

Sykes, L. R., W. R. McCann, and A. L. Kafka, Motion of Caribbean plate during last 7 million years and implications for earlier Cenozoic movements, *J. Geophys. Res., 87,* 10,656–10,676, 1982.

Toksöz, M. N., J. W. Minear, and B. R. Julian, Temperature field and geophysical effects of a downgoing slab, *J. Geophys. Res., 76,* 1113–1138, 1971.

C. DeMets, Department of Geology and Geophysics, University of Wisconsin at Madison, 1215 W Dayton St., Madison, WI 53706.

(Received May 4, 1992;
revised November 20, 1992;
accepted December 4, 1992.)